Chapter 8

The Onset Of Surface Oxide Decomposition

Using the atomistic thermodynamics approach it was possible to obtain a first, large scale picture of the possible stability of different (co-)adsorption structures on Pd(100) over a wide range of O and CO gas phase conditions. Nevertheless, for the here discussed system describing the catalytic CO oxidation at the Pd(100) surface, especially the assumption of a constrained thermodynamic equilibrium has to be qualified. The neglected CO_2 formation at the surface might have a significant influence on the stability of the different phases, since during the catalytic reaction the different subsystems, i.e. surface and gas phase, are most likely not in a full thermodynamic equilibrium as implied in the atomistic thermodynamics approach.

To explicitly include the on-going catalytic reaction at the surface, kinetic Monte Carlo (kMC) simulations (cf. Chapter 5) are performed. For the simulations the system is mapped onto a lattice to keep the number of possible processes manageable. At this point lattice-free kMC simulations based on *ab initio* input parameters would be computationally unfeasible. To include all phases identified in the afore discussed phase diagram (cf. Fig. 7.6), three different lattices would be needed to represent the three different parts indicated in Fig. 7.6, namely phases including the Pd(100) surface, the reconstructed $(\sqrt{5} \times \sqrt{5})R27^\circ$ surface oxide and the bulk oxide. Since the bulk oxide appears to be too unstable to play a role already in the atomistic thermodynamics approach and kinetic effects would be expected to reduce its stability region even further, it would be sufficient to consider only two lattices to model the catalytically active region representing the Pd(100) surface and the $(\sqrt{5} \times \sqrt{5})R27^\circ$ surface oxide structure. As discussed in Section 7.3 the area of catalytically relevant gas phase conditions ($p \approx 1\,\mathrm{atm}$, $T \approx 300 - 600\,\mathrm{K}$) is right at the boundary between phases involving the surface oxide structure and a CO covered Pd(100) surface. Thus, it would be necessary to also include the transition between the two phase, and respectively two kMC lattices, going from the Pd(100) surface to the $(\sqrt{5} \times \sqrt{5})R27^\circ$ surface oxide and vice versa. The reconstructed palladium layer in the surface oxide structure does, however, not only exhibit a different symmetry compared to the

Pd(100) surface, but it has also a different density, since there are only four Pd atoms in the $(\sqrt{5} \times \sqrt{5})R27°$ surface unit cell on five Pd(100) substrate atoms. Thus, the transition from the reconstructed surface oxide to the Pd(100) surface and vice versa appears to involve rather complex processes. An explicit modeling of both phases including a reversible transition between them is therefore extremely involved. In a first approach the present study will instead be restricted to only one phase. Starting at the catalytically relevant gas phase conditions in the stability region of the surface oxide, the focus will be on the stability of the $(\sqrt{5} \times \sqrt{5})R27°$ surface oxide structure under increasingly CO-rich gas phase conditions. Hence, in a first approach the kMC simulations are used to investigate the onset of surface oxide decomposition under reaction conditions and to compare these findings to the results obtained within the constrained atomistic thermodynamics approach. Focusing the kMC simulations on the $(\sqrt{5} \times \sqrt{5})R27°$ surface oxide structure only, a single lattice is sufficient to represent the different structures.

8.1 The Model

As shown in Fig. 7.3 the surface unit cell of the $(\sqrt{5} \times \sqrt{5})R27°$ structure contains 10 additional adsorption sites and 2 oxygen atoms in the upper hollow sites, which can also be removed or substituted by CO. These 12 sites can be reduced to 8, since the four additional hollow sites depicted in Fig. 7.3 are not stable adsorption sites, i.e. any adsorbate (O or CO) initial placed in such a hollow site moves to the corresponding bridge site upon relaxation. For the kMC lattice representing the $(\sqrt{5} \times \sqrt{5})R27°$ surface oxide the number of included sites can be further decreased, if the two sites of a corresponding site type (bridge, twofold by oxygen coordinated top, fourfold by oxygen coordinated top and hollow) within the surface unit cell are considered as being equivalent. Neglecting the small deviations in the energetics of such two like sites resulting from the symmetry of the underlying Pd(100) substrate (cf. Section 7.2), the $(\sqrt{5} \times \sqrt{5})R27°$ surface unit cell can be reduced to half its size, so that for the kMC lattice only four different sites need to be taken into account. In Fig. 8.1 a schematic illustration of the $(\sqrt{5} \times \sqrt{5})R27°$ surface is shown and the surface unit cell with the four adsorption sites as well as the respective kMC lattice are indicated.

The oxygen atoms in the surface oxide structure located below the reconstructed Pd layer at the interface to the Pd(100) substrate are treated as part of the kMC lattice (small red spheres in Fig. 8.1). This is done, since the reconstructed Pd layer shows already quite some distortion, if only the upper oxygen atoms are removed from their hollow sites. If in addition also the lower oxygen atoms are removed from the $(\sqrt{5} \times \sqrt{5})R27°$ surface oxide structure, the palladium atoms in the top layer are so much displaced, that they would not be properly described by the lattice depicted in Fig. 8.1 anymore.

As already mentioned above, the kMC simulations are performed to obtain a first insight into the stability of the surface oxide structure under reaction conditions. The

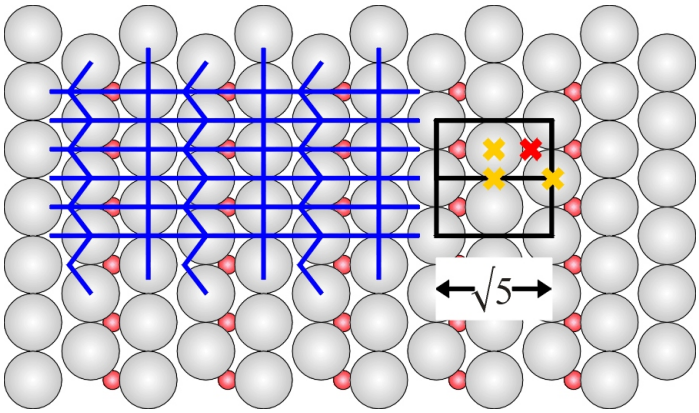

Figure 8.1: Schematic illustration of the $(\sqrt{5} \times \sqrt{5})R27°$ surface oxide structure. The surface unit cell as well as the adsorption sites and the respective kMC lattice are indicated. The large, grey spheres represent Pd atoms, the small, red ones O atoms. The two lower oxygen atoms of the surface oxide are included in the fixed kMC lattice, and not explicitly considered as flexible adsorbates.

simulations are thus started under gas phase conditions, where the surface oxide is a stable phase in the thermodynamic phase diagram (cf. Fig. 8.2). Keeping the oxygen pressure fixed at $p_{O_2} = 1\,\text{atm}$ the CO pressure is gradually increased from $p_{CO} = 10^{-5}\,\text{atm}$ to $p_{CO} = 10^{5}\,\text{atm}$ as indicated by the green arrows in Fig. 8.2 for three different temperatures of $T = 300\,\text{K}$, $T = 400\,\text{K}$ and $T = 600\,\text{K}$. Since the kMC simulations are restricted to a lattice representing the surface oxide, the onset of the surface oxide decomposition will be monitored by the occupation of the hollow sites (red cross in Fig. 8.1) by oxygen. If all hollow sites are occupied by oxygen the structure of the surface oxide is certainly maintained, a depletion of the oxygen atoms in the upper hollow sites will then be taken as indication of the onset of surface oxide decomposition. As discussed above, the entire transition from the surface oxide structure to the Pd(100) surface with increasing CO pressure (as expected from the thermodynamic phase diagram, cf. Fig. 8.2) can not be described within the chosen model.

The four different sites in the kMC lattice are arranged in a square, forming rows of alternating twofold top and hollow sites and rows of alternating bridge and fourfold top sites (the notation twofold and fourfold refers to the coordination of the top site palladium atoms by oxygen in the original surface oxide structure as shown in Fig. 7.3). Moving within one row from one site to the left or right neighboring site is not equivalent due to the lower oxygen atoms included in the lattice, whereas moving to the upper or lower neighboring site along a column is identical. This asymmetry in the lattice sites has to be explicitly considered in the determination of possible processes in the kMC simulation that involve more than one lattice site (dissociative adsorption, associative desorption, diffusion and reaction), as well as in the calculation of process rates that depend on the interactions between neighboring sites.

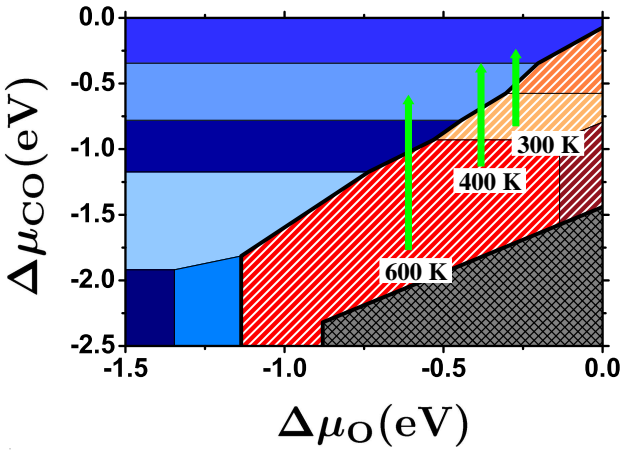

Figure 8.2: Thermodynamic phase diagram as obtained within the PBE exchange-correlation functional. The green bars indicate the pressure conditions of the kMC simulations for a temperature of $T = 300\,\mathrm{K}$, $T = 400\,\mathrm{K}$ and $T = 600\,\mathrm{K}$. The oxygen pressure is always fixed at $p_{O_2} = 1\,\mathrm{atm}$, while the CO pressure is varied between $10^{-5} \leq p_{CO} \leq 10^{5}\,\mathrm{atm}$.

Initial Considerations Of Sites

To investigate the relevance of the different sites in the kMC lattice representing the surface oxide, some initial tests are performed. Within these test simulations not all imaginable processes are included right from the beginning, but they are used to find out, which processes are important and which might be further coarse-grained in the setup of the final kMC simulation.

In a first test the hollow sites (marked by the red cross in Fig. 8.1) are not considered in the simulation, but simply taken as always completely filled by oxygen atoms, representing the original surface oxide structure. This structure is stable under a sufficiently high oxygen chemical potential and a low CO chemical potential, gas phase conditions which will be taken as starting point for studying the onset of the decomposition of the surface oxide structure (cf Fig. 8.2). Thus, in this first model the interactions of CO with the remaining adsorption sites will be evaluated under these initial conditions. Only 6 process types are considered in this model, which are the unimolecular adsorption and desorption of CO in the three remaining sites, namely the bridge, the twofold top and the fourfold top site. The corresponding rates are obtained by applying Eq. (5.12) and Eq. (5.23). A detailed discussion of all parameters entering the calculation of the different rates is given in Section 8.2 for the final kMC model. For the here described initial considerations a qualitative discussion appears to be sufficient. If no lateral interactions are included, the only difference between the three sites is the binding energy of the CO in each site, which influences the respective desorption rate. Consequently, the simulations yield that with increasing CO chemical potential, which is determined by the temperature and

pressure of the CO gas phase, first the bridge site, where the CO is bound most strongly (cf. Tab. 7.3), is occupied, then the twofold top site and finally the fourfold top site. Looking again at the DFT results it is found, that a structure with one CO in bridge and a second one in a twofold top site is not stable (cf. Page 93, and structure 18 in Appendix B.1), due to the strongly repulsive interactions between the two adsorbed molecules. In the kMC simulation this can be realized, if the adsorption of CO on the two twofold top sites neighboring a bridge site, that is already occupied by CO, is excluded, and vice versa. This restriction in the availability of adsorption sites leads to a preference in the occupation of bridge sites.

This preference becomes even more pronounced, if diffusion processes are included in a second test model. In addition to the 6 adsorption and desorption processes, 4 diffusion processes between the twofold top site and the bridge site (top2f $\leftrightarrow$ bridge) as well as between the fourfold top site and the bridge site (top4f $\leftrightarrow$ bridge) are considered. For the diffusion from either top site to the bridge site only a very small diffusion barrier is calculated ($\Delta E^{\mathrm{diff}}_{\mathrm{CO,top\rightarrow bridge}} < 0.1\,\mathrm{eV}$), whereas for the diffusion from the bridge to either top site this barrier is increased by the difference in binding energy between the two sites, so that $\Delta E^{\mathrm{diff}}_{\mathrm{CO,bridge\rightarrow top2f}} = 0.4\,\mathrm{eV}$ and $\Delta E^{\mathrm{diff}}_{\mathrm{CO,bridge\rightarrow top4f}} = 0.9\,\mathrm{eV}$. With these very small diffusion barriers effectively every CO molecule that is initially adsorbed on a top site will immediately diffuse to an empty neighboring bridge site at the temperatures of interest. Simulations within this model show, that the twofold top sites are then no longer significantly populated by CO anymore, but every CO initially adsorbed in a twofold top site now contributes to the occupation of the bridge sites. This can be explained, since the adsorption on the twofold top sites is only possible, if the neighboring bridge sites are empty, and thus also the diffusion is always possible. The fourfold top sites can still be populated, but only at a very high CO chemical potential, after all bridge sites are already occupied.

In the next step also the adsorption and desorption of oxygen on the three sites is considered, while still keeping all hollow sites occupied with oxygen atoms. Since the oxygen molecules adsorb dissociatively, always two empty sites are needed. This can in principle be realized in 6 different ways, 3 on two like sites (bridge–bridge, top2f–top2f, top4f–top4f) and 3 on mixed sites (bridge–top2f, bridge–top4f, top2f–top4f). Comparing to the DFT calculations, only the adsorption in two neighboring bridge sites appears reasonable, whereas all other combinations of adsorption sites result in energetically unstable geometries, i.e. the oxygen atoms do simply not bind to any of the top sites. Thus, also the diffusion of oxygen atoms from one bridge site to the next is not considered as possible process, since on a simple reaction coordinate the most likely transition state for this diffusion process is the unstable twofold top site. From these initial test simulations it can be seen, that the twofold top site has no relevance in the kMC model representing the surface oxide. For the oxygen it does not serve as a stable adsorption site at all, and for the CO it is basically only a transition state between two bridge sites. In the following simulations, the twofold top site is correspondingly not further considered.

With increasing CO chemical potential (following the green arrows in Fig. 8.2)

the surface oxide structure will become less stable. Thus, a 100 % occupation of the hollow sites by oxygen will not be justified anymore and processes including also the hollow sites have to be considered in a further test model. As additional processes, the CO adsorption and desorption at hollow sites, as well as the dissociative adsorption and associative desorption of oxygen involving hollow sites have to be considered. For the O_2 molecule there are now 3 different possibilities to adsorb, respectively desorb, namely the already included adsorption/desorption on/from bridge–bridge sites and in addition the adsorption/desorption in/from hollow–hollow and bridge–hollow sites. Running the simulations it turns out, that depending on the oxygen and CO gas phase conditions the hollow and bridge sites are either empty or occupied by O and/or CO, whereas the fourfold top sites can again only be occupied at very high CO chemical potential. In addition, the CO molecules adsorbed on a fourfold top site can now also diffuse to an empty hollow site, again with a computed very small barrier of $\Delta E^{\mathrm{diff}}_{\mathrm{CO,top4f\rightarrow hollow}} < 0.1\,\mathrm{eV}$, whereas the barrier for the diffusion from the hollow to the fourfold top site is rather large with $\Delta E^{\mathrm{diff}}_{\mathrm{CO,hollow\rightarrow top4f}} = 0.8\,\mathrm{eV}$. Thus, the fourfold top sites are only populated, if all bridge and all hollow sites are already filled. Moreover, the DFT calculations show, that the additional adsorption of CO on a fourfold top site, if all hollow and all bridge sites are occupied, leads to an unstable structure. This can be included in the kMC simulation by considering strongly repulsive interactions between the adsorbates. The fourfold top site is then never occupied, since as long as there are still empty, neighboring bridge or hollow sites, an adsorbed CO molecule will always diffuse there, and if all neighboring bridge and hollow sites are already occupied, the adsorption on the fourfold hollow sites is not possible anymore. Therefore, also the fourfold top site will not be explicitly considered in the following simulations, but always be treated as empty site.

The Final kMC Model

In the final kMC model only the bridge and the hollow sites are included, whereas the two top sites remain always unoccupied and are not available for any of the kMC processes. On this lattice containing only the bridge and the hollow site the following processes are considered:

1. Adsorption
   - CO bridge
   - CO hollow
   - O_2 bridge–bridge
   - O_2 hollow–hollow
   - O_2 bridge–hollow

2. Desorption
   - CO bridge
   - CO hollow
   - O_2 bridge–bridge
   - O_2 hollow–hollow
   - O_2 bridge–hollow
3. Diffusion
   - CO bridge $\leftrightarrow$ bridge
   - CO hollow $\leftrightarrow$ hollow
   - CO bridge $\leftrightarrow$ hollow
   - O hollow $\leftrightarrow$ hollow
   - O bridge $\leftrightarrow$ hollow
4. Reaction (modeled as associative desorption)
   - O hollow + CO bridge $\leftrightarrow$ CO_2
   - O bridge + CO hollow $\leftrightarrow$ CO_2

This list contains the most obvious kinds of processes with respect to the chosen lattice. It can not be excluded, that other, more complicated processes might have some influence on the here discussed system. Nevertheless, the suggested setup does at least provide a reasonable starting point.

8.2 The Rates

For every process listed in the previous Section a process rate has to be determined. The general derivation of the rates for the four different process types (adsorption, desorption, diffusion and reaction) is given in Section 5.2. Here, the different parameters entering the rates for the simulation of the surface oxide are discussed.

8.2.1 Adsorption

To determine the impingement rate entering Eq. (5.12) the only parameters, that are system specific, are the mass of the impinging gas phase molecules ($m_{O_2} = 5.31 \cdot 10^{-26}\,\mathrm{kg}$ and $m_{CO} = 4.65 \cdot 10^{-26}\,\mathrm{kg}$) and the surface area, whereas temperature and pressure are varied for the different simulations. According to the model described in the previous Section the surface area corresponds to half the surface unit cell of the $(\sqrt{5} \times \sqrt{5})R27^\circ$ surface oxide, i.e. $A = 1/2\, A_{(\sqrt{5}\times\sqrt{5})R27^\circ} = 19.47\,\text{Å}^2$. The

determination of the local sticking coefficient $\tilde{S}_{i,st}$, on the other hand, is much more complicated. As discussed in Section 5.2.2 for a proper determination of $\tilde{S}_{i,st}$ the full, high-dimensional potential energy surface (PES) for the adsorption process is needed. On this PES molecular dynamics (MD) simulations have to be performed for a statistically relevant number of trajectories [87]. For the present study, though, only a first, rough order of magnitude estimate of the local sticking coefficient is needed. Thus, it is first determined, if there are any significant adsorption barriers along the minimum energy pathway (MEP) for any of the five different adsorption processes (cf. Eq. (5.16)). For the CO molecule this is done by vertically lifting the CO in an upright geometry from a bridge or a hollow site. The energy of the whole system is then minimized with respect to all other degrees of freedom for different heights of the CO molecule above its adsorption site. For neither of the two sites a barrier is found along this desorption, respectively adsorption, pathway. For the dissociative adsorption of the oxygen molecule a PES is mapped out, in which the energy is given as a function of the bond length between the two O atoms and the height of their center of mass above the surface. The lateral position of the center of mass above the surface, as well as the orientation of the O_2 molecule are kept fixed (i.e. there is no rotation of the molecule around its center of mass). Due to its shape such a plot is also called an *elbow plot*. Since there are only two hollow sites within the $(\sqrt{5} \times \sqrt{5})R27^\circ$ surface unit cell, a lifting of two oxygen atoms would correspond to a complete removal of all upper oxygen atoms in the surface oxide structure due to the periodic supercell setup of the DFT calculations. Thus, these calculations are performed in a (1×2)-$(\sqrt{5} \times \sqrt{5})R27^\circ$ surface unit cell. For the O_2 adsorption on neighboring hollow sites the energy decreases smoothly along the elbow plot apart from a small molecular physisorption well $\sim 0.3\,\text{Å}$ above the optimal adsorption site of the dissociated oxygen atoms. The dissociation of an O_2 molecule in this particular orientation along the respective elbow plot can therefore be considered as non-activated. A similar plot is also found for the O_2 adsorption in neighboring bridge–hollow sites and equivalent results are also expected for the adsorption in two neighboring bridge sites. Since in these calculations only one molecular orientation at a fixed lateral position within the surface unit cell is evaluated for each adsorption process, this is by far not enough to describe the full, high-dimensional PES underlying any of the adsorption processes. Nevertheless, if there exists one barrier free entrance channel connecting the gas phase and the adsorbed state, then also the maximum barrier along the MEP must be zero. As a result, the adsorption barrier in Eq. (5.16) is set to zero, $\Delta E^{\text{ads}} = 0$, for all five adsorption processes.

As a next parameter the factor $f_{i,st}^{\text{ads}}$ is considered. As already explained in Section 5.2.2 this factor reduces the number of impinging gas phase particles by the fraction, that is not traveling along the MEP and might therefore be reflected at some higher energy barrier along a different pathway. Since the here performed simulations are in a temperature range of $T = 300 - 600\,\text{K}$, where the impinging gas phase molecules can still be considered as rather slow, it is assumed, that the molecules are rather efficiently steered along the barrier free pathways [87] and thus the value of

f^{ads} is approximated by $f^{\mathrm{ads}} \approx 1$ for all five adsorption processes. Trying out a few trajectories on the barrier free PESs does indeed lead to the conclusion that the local sticking coefficient can roughly be approximated by $\tilde{S}_{i,st} \approx 1$.

The last parameter is the size of the active area $A_{i,st}$. Following the previous discussion, there is no argument, why either of the two adsorption sites should be favored. The most obvious choice is then to equally divide the surface area A among the different adsorption sites, yielding $A_{\mathrm{CO,br}} = A_{\mathrm{CO,hol}} = 1/2A$ for the adsorption of CO and $A_{\mathrm{O_2,br-br}} = A_{\mathrm{O_2,hol-hol}} = A_{\mathrm{O_2,br-hol}} = 1/3A$ for the adsorption of O_2. Thus, also the adsorption of molecules impinging on top sites and immediately diffusing to neighboring bridge or hollow sites is included in an effective way.

Using these approximations for the different parameters the calculation of the rates for the five different adsorption processes is straightforward. From the above discussion, though, it becomes clear, that there are still some uncertainties in the rates due to the well reasoned, but still approximate determination of parameters. This uncertainty will be considered in the discussion of the simulation results at the end of this Chapter.

8.2.2 Desorption

The desorption rates are connected to the adsorption rates by the detailed balance criterion (cf. Eq. 5.18). Thus, having determined the adsorption rates the corresponding desorption rates can be obtained by applying Eq. (5.23). In a first approach the vibrational partition function in the adsorbed state is set to unity, $z^{\mathrm{vib}}_{i,st} = 1$, for all desorption processes. In the gas phase the vibrational partition function of oxygen and CO can very well be approximated by unity over the here investigated temperature range ($T = 300 - 600\,\mathrm{K}$), i.e. only the first vibrational state is excited. In the adsorbed state this might be changed, though, due to the lower frequency modes resulting from the adsorbate–substrate bond, which could then lead to a somewhat larger partition function, $z^{\mathrm{vib}}_{i,st} > 1$.

The second parameter, that is needed to determine the desorption rate, is the binding energy. The binding energies of oxygen and CO in the bridge and hollow sites do in general depend on the interaction between neighboring sites. Thus, a lattice gas Hamiltonian (LGH) is set up (cf. Section 5.1.2) to determine the binding (resp. desorption) energies during the simulation using Eq. (5.8). From the DFT calculations it becomes obvious that the interactions between the adsorbates do not extend beyond the $(\sqrt{5} \times \sqrt{5})R27^\circ$ surface unit cell for the here assumed level of accuracy of the binding energies, i.e. the change in the binding energies is $< 0.1\,\mathrm{eV}$ (cf. Appendix B.2). Consequently, in the LGH only nearest neighbor pair interactions

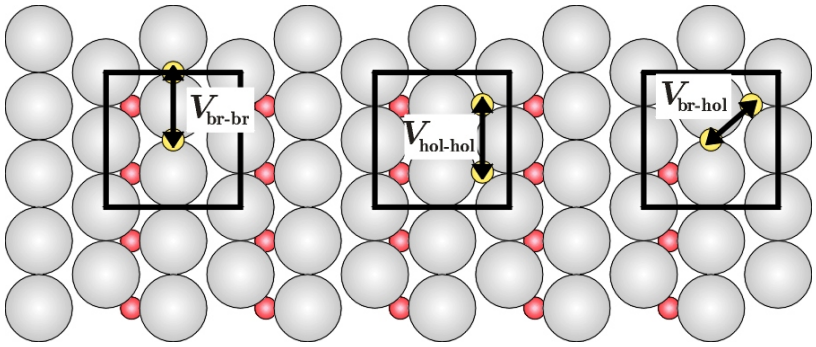

Figure 8.3: First nearest neighbor pair interactions between adsorbates on the $(\sqrt{5}\times\sqrt{5})R27°$ surface oxide. An adsorbate sitting in a bridge site does only interact with adsorbates in right neighboring hollow sites, whereas the left neighboring hollow sites are too far away. Large, grey spheres represent Pd atoms, small, red spheres oxygen atoms included in the kMC lattice and small yellow spheres adsorbed O and/or CO.

are included

$$\begin{aligned} H = &\sum_i \left[n_{\mathrm{O},i} E^0_{\mathrm{O},i} + n_{\mathrm{CO},i} E^0_{\mathrm{CO},i} \right] \\ &+ \sum_{ij} \left[V_{\mathrm{O-O},ij}\, n_{\mathrm{O},i}\, n_{\mathrm{O},j} + V_{\mathrm{CO-CO},ij}\, n_{\mathrm{CO},i}\, n_{\mathrm{CO},j} + V_{\mathrm{O-CO},ij}\, n_{\mathrm{O},i}\, n_{\mathrm{CO},j} \right] \quad , \end{aligned} \tag{8.1}$$

where j only runs over the corresponding neighboring sites. The binding energy of a CO molecule in a site i is then e.g. given by

$$\begin{aligned} E^{\mathrm{bind}}_{\mathrm{CO},i} &= H(n_{\mathrm{CO},i}=1) - H(n_{\mathrm{CO},i}=0) \\ &= E^0_{\mathrm{CO},i} + 2\sum_j \left[V_{\mathrm{CO-CO},ij}\, n_{\mathrm{CO},j} + V_{\mathrm{O-CO},ij}\, n_{\mathrm{O},j} \right] \quad . \end{aligned} \tag{8.2}$$

Equivalently, the binding energy of an oxygen atom is calculated. For the associative desorption of an O_2 molecule, respectively, two neighboring sites are depleted, which can be expressed similarly using the LGH. As shown in Fig. 8.3 the first nearest neighbor pair interactions correspond to interactions between two neighboring bridge sites, two neighboring hollow sites and between neighboring bridge and hollow sites. Thus, there are six different interaction parameters between like species ($V_{\mathrm{O-O,br-br}}$, $V_{\mathrm{O-O,hol-hol}}$, $V_{\mathrm{O-O,br-hol}}$, $V_{\mathrm{CO-CO,br-br}}$, $V_{\mathrm{CO-CO,hol-hol}}$, $V_{\mathrm{CO-CO,br-hol}}$) and four different between unlike species ($V_{\mathrm{O-CO,br-br}}$, $V_{\mathrm{O-CO,hol-hol}}$, $V_{\mathrm{O-CO,br-hol}}$, $V_{\mathrm{O-CO,hol-br}}$). Together with the four on-site energies there is thus a total of 14 parameters, which have to be determined for the LGH. The parameters can be obtained by fitting to DFT results (cf. Section 5.1.2). The on-site terms can either be determined in the fitting procedure, or they are taken from a low coverage limit. Calculating the on-site energies in a low-coverage limit is often preferred, if long-range interactions are not expected to have an important contribution. A direct evaluation of the on-site terms

$E^0_{\mathrm{O,br}}$	$E^0_{\mathrm{O,hol}}$	$E^0_{\mathrm{CO,br}}$	$E^0_{\mathrm{CO,hol}}$
-0.51	-1.95	-1.40	-1.92
$V_{\mathrm{O-O,br-br}}$	$V_{\mathrm{O-O,hol-hol}}$	$V_{\mathrm{O-O,br-hol}}$	
0.08	0.07	0.08	
$V_{\mathrm{CO-CO,br-br}}$	$V_{\mathrm{CO-CO,hol-hol}}$	$V_{\mathrm{CO-CO,br-hol}}$	
0.08	0.13	0.14	
$V_{\mathrm{O-CO,br-br}}$	$V_{\mathrm{O-CO,hol-hol}}$	$V_{\mathrm{O-CO,br-hol}}$	$V_{\mathrm{O-CO,hol-br}}$
0.06	0.11	0.13	0.12

Table 8.1: Four on-site energies E and ten first nearest neighbor interaction parameters V for the lattice gas hamiltonian describing the adsorption of O and CO in hollow and bridge sites of the surface oxide. All values are in eV.

can then become favorable, since the on-site terms are usually at least one order of magnitude larger than the interaction parameters, but within the fitting procedure all parameters will have the same relative error, which correspondingly leads to a much larger absolute error in the on-site terms. For the surface oxide structure, though, only the on-site energies for the hollow sites could be determined from a low coverage limit. Occupying only one bridge site leaving both hollow sites empty within the $(\sqrt{5}\times\sqrt{5})R27^\circ$ surface unit cell leads again to a strong displacement of the atoms in the reconstructed palladium layer. It was therefore not possible to obtain reliable on-site energies for O or CO in bridge position in a low coverage limit. Consequently, in the present work the interaction parameters as well as the on-site energies are included in the fitting procedure. To fit the 14 parameters 29 different configurations of O and/or CO in bridge and hollow sites are calculated within the $(\sqrt{5}\times\sqrt{5})R27^\circ$ surface unit cell and the respective energy of each configuration is expressed in term of a lattice gas expansion (for a detailed discussion cf. Appendix C) . Since in the kMC model the lower oxygen atoms are part of the lattice, the energies of the different configurations are calculated with respect to the *empty* lattice, i.e.

$$\Delta E = E_{\mathrm{O,CO@}(\sqrt{5}\times\sqrt{5})R27^\circ} - E_{(\sqrt{5}\times\sqrt{5})R27^\circ-2\mathrm{O}} - N_{\mathrm{O}}1/2E^{\mathrm{tot}}_{\mathrm{O_2}} - N_{\mathrm{CO}}E^{\mathrm{tot}}_{\mathrm{CO}} \quad , \qquad (8.3)$$

where $E_{(\sqrt{5}\times\sqrt{5})R27^\circ-2\mathrm{O}}$ corresponds to the surface oxide structure without the two upper oxygen atoms (structure 117 in Appendix B.1). All energies are calculated using the PBE as approximation to the exchange-correlation functional. Using the 29 different configurations the 14 parameters are obtained by a least-square fit. In Tab. 8.1 the four on-site energies and the 10 interaction parameters are listed. The fitted on-site energies of O or CO in hollow sites compare rather well to the binding energies in the low coverage limit, $E^{\mathrm{bind}}_{\mathrm{O,hol}} = -1.83\,\mathrm{eV}$ and $E^{\mathrm{bind}}_{\mathrm{CO,hol}} = -1.92\,\mathrm{eV}$, within the here aspired level of accuracy. All interaction parameters are positive reflecting the purely repulsive interaction between neighboring adsorbates. Comparing the on-site energies it can be seen, that both O and CO prefer the hollow site. If competing

for the same site, though, the oxygen binds more strongly on the hollow site, whereas the CO is more strongly bound on the bridge site. Including the repulsive interactions this trend is maintained for all possible configurations.

Using these parameters the binding energy of every adsorbate can be evaluated for any random configuration by utilizing Eq. (8.2), and the respective desorption rate can be calculated via Eq. (5.23).

8.2.3 Diffusion

To calculate the diffusion rates by applying Eq. (5.28) the transition states along the diffusion pathways are needed. For the diffusion from one bridge site to a neighboring one, the transition state is simply given by the twofold top site. The transition state for the diffusion from a hollow to a neighboring bridge or hollow site is more difficult to define, which is mainly due to the mobility of the topmost Pd layer, if an adsorbate is moved away from a hollow site. If, e.g., an oxygen atom sitting in a hollow site is displaced in y-direction, the topmost Pd layer will follow this displacement, so that, if all but the oxygen y-coordinate are relaxed, the whole reconstructed surface oxide layer is simply shifted with respect to the underlying substrate, whereas the displaced O atom remains perfectly in the hollow site. It has been shown previously that the reconstructed surface oxide layer can be shifted over the Pd(100) substrate rather easily, exhibiting an energetic corrugation of $< 0.65\,\mathrm{eV}$/unit cell [144]. Compared to the binding energy of an oxygen atom in hollow site ($E^{\mathrm{bind}}_{\mathrm{O,hol}} = -1.83\,\mathrm{eV}$) this is rather small. Thus, it becomes energetically more favorable to shift the surface oxide layer instead of displacing an oxygen atom from a hollow site when using smaller (periodic boundary conditions) surface unit-cells. In a larger surface unit cell, though, the difference in energy that is needed to shift the surface oxide layer compared to displacing one oxygen atom from a hollow site becomes smaller and eventually in a huge supercell the effect would vanish. Unfortunately, doubling the surface unit cell in x- or y-direction appears not to be sufficient to prevent the shifting of the reconstructed palladium layer and calculations in even larger surface unit cells were computational too demanding at this time.

To obtain at least approximate values for the diffusion barriers the xy-coordinates of the palladium atoms in the surface oxide layer are additionally fixed during the transition state search. The resulting values of the diffusion barriers are listed in Tab. 8.2. They are calculated within the $(1 \times 1) - (\sqrt{5} \times \sqrt{5})R27^\circ$ surface unit cell, with both hollow sites occupied by O (CO diffusion bridge $\rightarrow$ bridge, structure 1 in Appendix B.1), only one hollow site occupied by O (CO/O diffusion bridge $\rightarrow$ hollow, structures 29 $\rightarrow$ 28 and 106 $\rightarrow$ 105) and one hollow site occupied by CO/O (CO/O diffusion hollow $\rightarrow$ hollow, structures 60 and 113). In this structural setup, the initial and final state for the diffusion between like sites have the same energy, as shown in the left part of Fig. 8.4. For the diffusion between unlike sites or like sites with different nearest neighbor interactions, though, the energy of the initial and final state well differ. Here, the values listed in Tab. 8.2 are taken as minimum values for the

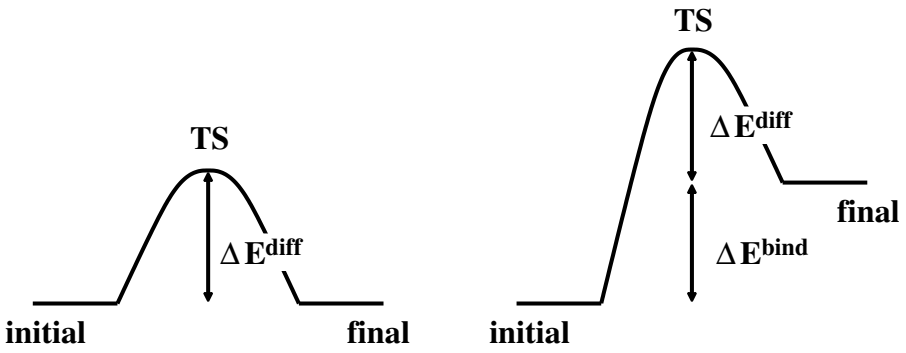

Figure 8.4: Schematic illustration of the diffusion barrieres between energetically like and unlike sites.

	$\Delta E^{\mathrm{diff}}_{\mathrm{br}\to\mathrm{br}}$	$\Delta E^{\mathrm{diff}}_{\mathrm{hol}\to\mathrm{hol}}$	$\Delta E^{\mathrm{diff}}_{\mathrm{br}\to\mathrm{hol}}$
O	–	1.4	0.1
CO	0.4	0.6	0.3

Table 8.2: Barriers for the diffusion between the different sites within the $(\sqrt{5}\times\sqrt{5})R27^\circ$ surface unit cell. All values are in eV.

diffusion barriers, i.e. if the final state has the same or a lower energy than the initial state the diffusion barrier is fixed to this value. Only if the final state is higher in energy the difference in binding energies between the initial and final state is added to the diffusion barrier (right part in Fig. 8.4) to ensure that the detailed balance criterion is fulfilled for the two time reversed diffusion processes.

To determine the remaining factor $f^{\mathrm{diff,TST}}_{i,st\to st'}$ in Eq. (5.29) it is assumed, that the vibrational partition functions of the adsorbate in the initial and at the transition state are approximately the same, i.e. $z^{\mathrm{vib}}_{i,st} \approx z^{\mathrm{vib}}_{i,st\to st',\mathrm{TS}}$, yielding $f^{\mathrm{diff,TST}}_{i,st\to st'} \approx 1$.

In this way, the rates of the different diffusion events were calculated for all possible system configurations. Since it turns out that the diffusion processes do not have any significant influence on the results of the kMC simulations and can actually be neglected, also the uncertainties in the rates introduced by the described approximations are irrelevant for the discussion of the results.

8.2.4 Reaction

The rates for the reaction of adsorbed O and CO to form CO_2 is calculated using Eq. (5.31). To determine the reaction barrier $\Delta E^{\mathrm{reac}}_{\mathrm{O+CO}\to\mathrm{CO_2}}$ the respective transition states have to be determined for the two included reactions O hollow + CO bridge and O bridge + CO hollow. Here, the transition state is searched by mapping out a 2-dimensional potential energy surface (PES), where the energy is plotted as a function

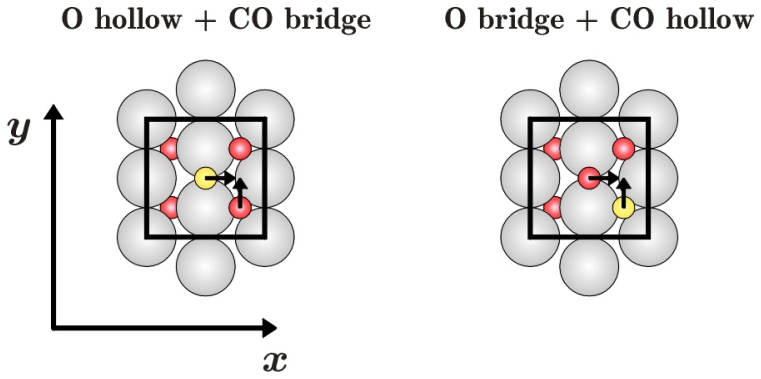

Figure 8.5: Geometries for the transition state search for the reaction of O hollow + CO bridge (left) and O bridge + CO hollow (right). The x- respectively y-coordinate of the O (red spheres) resp. C (yellow spheres) atom are fixed along the black arrows. To avoid a lateral shifting of the complete surface oxide structure with respect to the underlying Pd(100) substrate the xy-coordinates of the palladium atoms in the reconstructed layer (grey spheres) are additionally fixed.

of the x-coordinate of the CO/O in bridge site and the y-coordinate of the O/CO in hollow site with respect to their initial position within the $(\sqrt{5} \times \sqrt{5})R27°$ surface unit cell as shown in Fig 8.5. All other degrees of freedom are completely relaxed. As already mentioned in the previous Section, the topmost Pd layer shows a rather high mobility with respect to a lateral shift along the substrate, when using small surface unit cells. When mapping out the PES in a (1×1) surface unit cell the effect appears to be again so large, that it is not possible to find a proper transition state. Also in $(1 \times 2)-$ and $(2 \times 1) - (\sqrt{5} \times \sqrt{5})R27°$ surface unit cells a shifting of the surface oxide layer was still present, while calculations in even larger cells are at this time unfortunately prohibitive.

To circumvent this problem a two-step approach is chosen to obtain at least approximate values for the reaction barriers. In a first step the xy-coordinates of the Pd atoms in the reconstructed surface oxide layer are additionally fixed (cf. Fig. 8.5) and the energy is only minimized with respect to the remaining coordinates. The resulting PESs are shown in Fig. 8.6. The respective transition states are marked by a yellow circled cross. The barrier for the reaction O hollow + CO bridge is rather high with $\Delta E^{\mathrm{reac}}_{\mathrm{Ohol+CObr}} = 1.3\,\mathrm{eV}$, whereas for the reaction of O bridge + CO hollow only a barrier of $\Delta E^{\mathrm{reac}}_{\mathrm{Obr+COhol}} = 0.6\,\mathrm{eV}$ is found. In a second step the transition state geometries are now also relaxed with respect to the xy-coordinates of the topmost palladium atoms, while fixing all three coordinates of the reactants O and CO, to release some of the lateral stress that was induced by fixing the lateral positions of the palladium atoms in the first step. In this second relaxation step the barrier of the first reaction (O hollow + CO bridge) is lowered by $\sim 0.4\,\mathrm{eV}$ giving $\Delta E^{\mathrm{reac}'}_{\mathrm{Ohol+CObr}} = 0.9\,\mathrm{eV}$, whereas for the second reaction the effect is much smaller, yielding $\Delta E^{\mathrm{reac}'}_{\mathrm{Obr+COhol}} = 0.5\,\mathrm{eV}$. Also the remaining, maximum forces on the fixed O and C atoms are rather moderate, $\sim 46\,\mathrm{mRy/bohr}$ for the first reaction and $\sim 20\,\mathrm{mRy/bohr}$ for the second reaction.

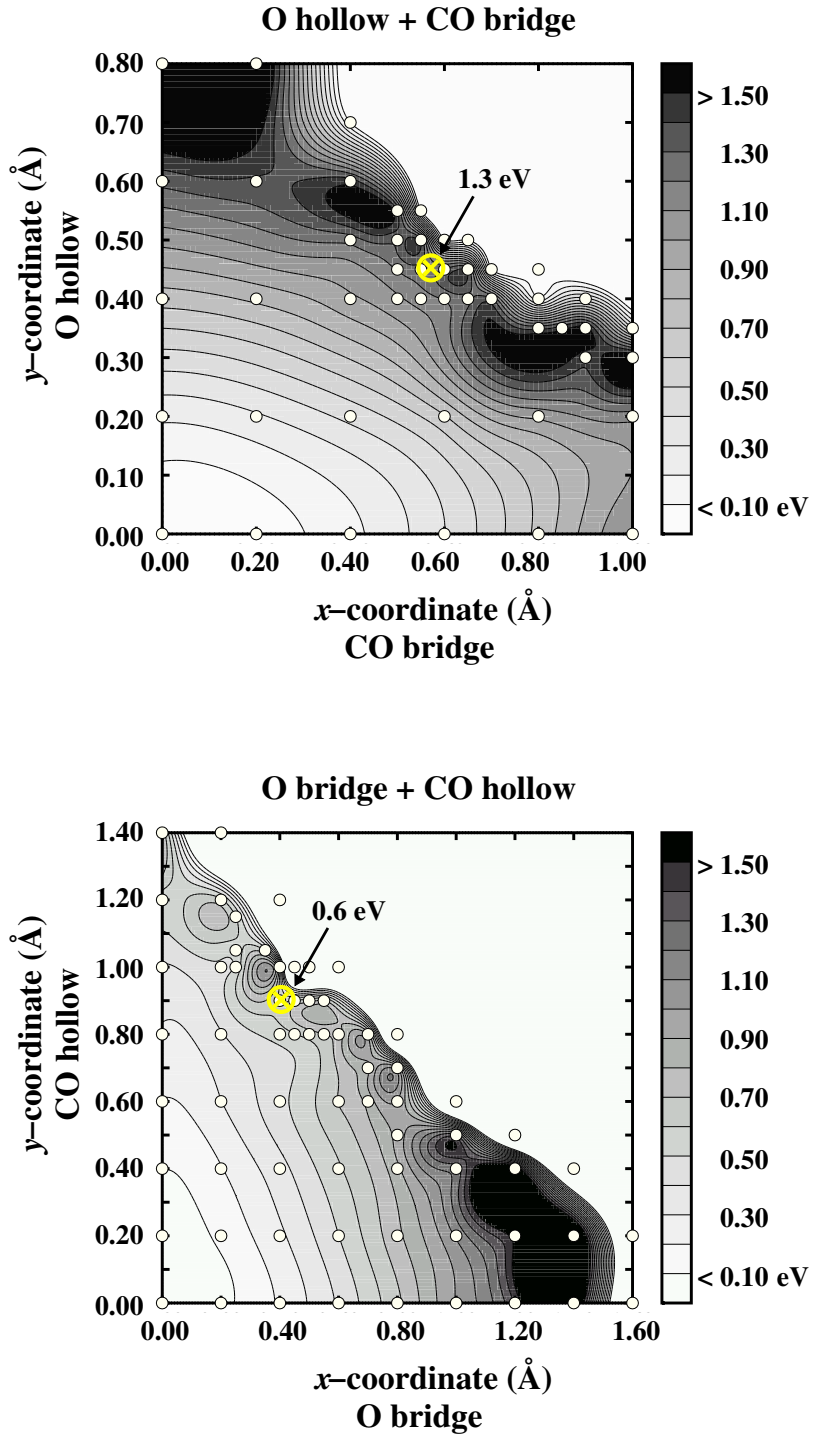

Figure 8.6: Potential energy surfaces for the reaction of O hollow + CO bridge (top) and O bridge + CO hollow (bottom). The x- and y-coordinates are given with respect to the initial adsorption site in the surface unit cell. The actually calculated points are indicated by white circles. The energy zero corresponds to the initial configuration. The transition state is marked by a yellow circled cross. All energies are in eV.

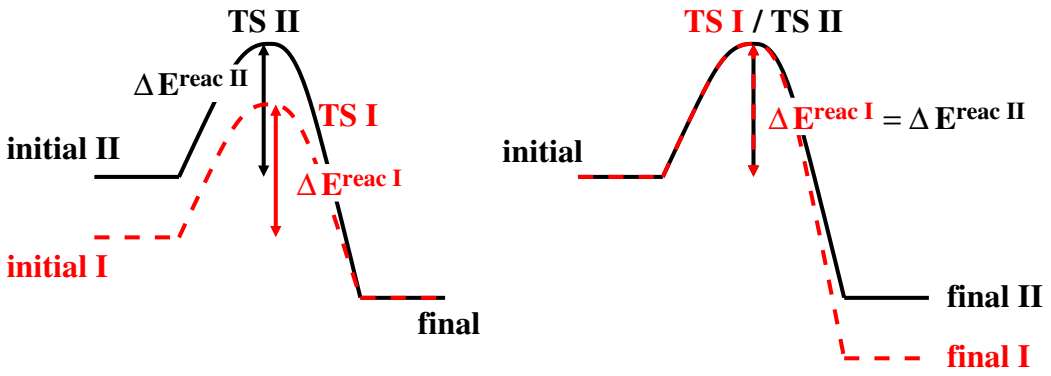

Figure 8.7: Schematic illustration of the reaction barrieres for different initial and final states. Here, the transition state is dominated by the initial state, thus the reaction barriers maintain constant.

Thus, the transition states obtained within this two step approach can be considered as good approximations to the real transition states. Due to the constraints in the degrees of freedom the energies of the real transition states can be expected to be slightly lower than the here presented values, but in any case they will not lead to higher barriers.

For the reaction processes the energies of the initial, transition and final states will be influenced by the nearest neighbor interactions. Since the geometries of the transition states are still quite similar to the initial states, it is assumed that the energies of the transition states will be equally influenced by these interactions. Thus, the energy differences between the initial and transition states will not be affected by the nearest neighbor interactions, i.e. the reaction barriers will be constant with respect to different configurations (cf. Fig. 8.7). The energies of the final states, though, containing the desorbed CO_2 are not considered to have any influence on the transition states.

The remaining prefactor $f^{\mathrm{reac,TST}}$ is again given as the ratio of the partition functions in the transition and initial state. As already mentioned above, for the reaction processes the initial and transition states are considered as similar leading also to comparable partition functions, so that the prefactor is approximated by $f^{\mathrm{reac,TST}} \approx 1$ for both reaction processes.

Since the reaction processes are modeled as associative desorption (cf. Section 5.2.5), the corresponding time reversed process is the dissociative adsorption of CO_2 into the respective adsorption sites. The activation barrier for such a process can be obtained from the reaction barrier and the corresponding binding energies using Eq. (5.27). Since the energy of CO_2 in the gas phase is much lower than the energy of adsorbed O and CO, the activation barriers for the CO_2 adsorption are rather high. Taking even the lowest resulting barrier of $\Delta E^{\mathrm{ads}}_{\mathrm{CO_2,br-hol}} = 1.4\,\mathrm{eV}$ and a temperature of $T = 600\,\mathrm{K}$, the local sticking coefficient (cf. Eq. 5.16) would still only be of the order of 10^{-12}. Even if the CO_2 generated at the surface is not readily transported away, and a no-

ticeable CO_2 pressure would build up, the readsorption of CO_2 will be negligible due to this very low sticking coefficient compared to the non-activated adsorption of O_2 and CO.

8.3 The Simulations

After having setup the kMC lattice and determining the different processes and their respective process rates, the simulations can be performed. This is done in two steps, starting with simulations, where only the adsorption, desorption and diffusion processes are considered, whereas the reaction processes are excluded. This reflects then the same situation as in the constrained atomistic thermodynamics approach, where likewise the formation of CO_2 was not considered. In the second step then, also the reaction events are included, hereby focusing on a change in the stability of the surface oxide structure.

8.3.1 Reproducing The Constrained Equilibrium

Within the kMC simulation it is possible to follow the evolution of the modeled system starting from some random initial state. If the simulation runs long enough, the system should eventually always reach the same so-called steady-state. For the here discussed problem the steady-state of the system is reached, if the average surface population becomes constant. If no reaction events are included in the simulation, the occupation at the surface under steady-state conditions corresponds then to a surface in a constrained thermodynamic equilibrium with an oxygen and CO gas phase, just as described by the atomistic thermodynamics approach, but including the effect of configurational entropy in the considered adsorption sites. The results obtained in the kMC simulations can therefore directly be compared to the atomistic thermodynamics results discussed in Section 7.3, which also provides a possibility to validate the chosen kMC setup. As it was discussed above, the kMC model does only represent the structure of the $(\sqrt{5} \times \sqrt{5})R27^\circ$ surface oxide, i.e. the kMC results can only be compared to the part of the phase diagram, where the surface oxide structure is stable (red/orange-white striped phases in Fig. 7.6).

The average occupation of a site-type st by a species i is calculated as

$$\overline{\Theta}_{i,st} = \frac{\sum_k \Theta_{i,st,k} \cdot \Delta t_k}{\sum_k \Delta t_k} \quad , \tag{8.4}$$

where Δt_k is the time step of the k's Monte Carlo move (cf. Eq. (5.6)), i.e. the longer the system is in a specific state, the more this state will contribute to the average occupation. Depending on the initial configuration and the chosen temperature and pressure conditions the steady-state is reached at quite different times. Thus, to begin with the simulations are run for a fixed number of kMC steps to obtain an order of magnitude estimate of the real time interval. But also the number of kMC steps

300K						
p_{O_2}	p_{CO}	$\overline{\Theta}_{O,hol}$	$\overline{\Theta}_{CO,hol}$	$\overline{\Theta}_{O,br}$	$\overline{\Theta}_{CO,br}$	phase diagram
10^{-10}	10^{-10}	1.00	0.00	0.00	0.00	surface oxide
10^{-5}	10^{-10}	1.00	0.00	0.00	0.00	surface oxide
10^{-5}	10^{-5}	1.00	0.00	0.00	0.50	surface oxide + CO bridge
1	10^{-10}	1.00	0.00	0.00	0.00	surface oxide
1	10^{-5}	1.00	0.00	0.00	0.50	surface oxide + CO bridge
1	1	1.00	0.00	0.00	1.00	surface oxide + 2 CO bridge
10^{10}	10^{-10}	steady-state not reached				surface oxide + O bridge
10^{10}	1	steady-state not reached				surface oxide + 2 CO bridge
600K						
p_{O_2}	p_{CO}	$\overline{\Theta}_{O,hol}$	$\overline{\Theta}_{CO,hol}$	$\overline{\Theta}_{O,br}$	$\overline{\Theta}_{CO,br}$	phase diagram
1	1	1.00	0.00	0.00	0.00	surface oxide
10^3	1	1.00	0.00	0.00	0.00	surface oxide
10^3	10^3	1.00	0.00	0.00	0.50	surface oxide + CO bridge
10^6	1	1.00	0.00	0.10	0.01	surface oxide
10^6	10^3	1.00	0.00	0.00	0.50	surface oxide + CO bridge
10^6	10^6	1.00	0.00	0.00	0.99	surface oxide + 2 CO bridge
10^{10}	1	1.00	0.00	0.49	0.00	surface oxide + O bridge
10^{10}	10^6	1.00	0.00	0.00	0.99	surface oxide + 2 CO bridge

Table 8.3: Average occupation of hollow and bridge sites by oxygen and CO for various pressures at $T = 300\,\mathrm{K}$ and $600\,\mathrm{K}$ representing the stability range of the surface oxide structure as determined within the atomistic thermodynamics approach. In the last column the corresponding thermodynamically most stable structure is listed. All pressures are in atm.

necessary to reach the steady-state can vary significantly. Therefore, the convergence of the average surface population was checked carefully for every initial surface configuration and (T, p)-conditions, by running the simulation for different numbers of kMC steps and averaging over different time intervals.

For the simulations a (20×20) lattice containing 100 bridge and 100 hollow sites is used. Test calculations are performed also for larger lattice sizes up to a (50×100) lattice, but no noticeable differences regarding the steady-state populations were observed. The simulations are performed at two different temperature $T = 300\,\mathrm{K}$ and $T = 600\,\mathrm{K}$ and pressure ranges of oxygen and CO of $p_{O_2} = 10^{-10} - 10^{10}\,\mathrm{atm}$ and $p_{CO} = 10^{-10} - 1\,\mathrm{atm}$, respectively $p_{O_2} = 1 - 10^{10}\,\mathrm{atm}$ and $p_{CO} = 1 - 10^{6}\,\mathrm{atm}$ for the higher temperature, to cover the whole stability region of the surface oxide considered in the atomistic thermodynamics approach discussed before. As initial configurations a completely empty lattice, and a lattice, where all hollow sites are occupied by oxygen, are chosen. The steady-state is reached in almost all simulations, nicely reproducing the surface oxide configurations shown in the thermodynamic phase diagram (Fig. 7.6), except for very high oxygen and CO pressures at $T = 300\,\mathrm{K}$. Under these conditions, the adsorption/desorption process of O_2 in two neighboring bridge sites is so fast, that it actually takes place on a different time scale compared to

all other processes. In this part of the thermodynamic phase diagram the surface oxide having two CO adsorbed in bridge site is the most stable one, i.e. in the kMC simulation all hollow sites should be occupied by oxygen and all bridge sites by CO. Running the simulation at $T = 300\,\mathrm{K}$ the hollow sites are found to be 100 % occupied by oxygen, whereas the occupation of the bridge sites varies depending on the initial configuration due to the predominance of the O_2 adsorption/desorption processes. Even with longest simulation times it was not possible to reach the steady-state situation. At $T = 600\,\mathrm{K}$, though, and gas phase conditions representing the same oxygen and CO chemical potentials as before for $T = 300\,\mathrm{K}$, the system reaches its steady-state rather quickly, so that also this part of the phase diagram can be reproduced.

Repeating the simulations without considering any of the diffusion processes does not change any of the discussed results. Since the hollow sites are almost always completely filled by oxygen, the only relevant diffusion process is the diffusion of CO from one bridge site to a neighboring one. This does, however, not have a noticeable influence on the average surface population. Since the diffusion processes do not appear to be important and can actually be excluded from the kMC simulation, also the uncertainties in the diffusion rates due to the only approximate transition states do not have any influence on the discussed results.

It can be concluded that using the above introduced kMC model without any reaction processes the 4 different surface oxide phases appearing in the thermodynamic phase diagram are well reproduced. Depending on the temperature and pressure conditions the bridge site is either empty, 50 % occupied by O, 50 % occupied by CO or completely filled by CO, whereas the hollow site is always occupied by oxygen (cf. Tab. 8.3).

8.3.2 Onset Of Surface Oxide Decomposition Under Reaction Conditions

To evaluate the stability of the surface oxide structure under reaction conditions the two reaction processes are now also included into the kMC simulations. As already mentioned above the simulations can not be performed over the whole range of oxygen and CO gas phase conditions evaluated in the thermodynamic phase diagram, since the kMC lattice can only represent the structure of the surface oxide. Thus, a restructuring of the surface palladium atoms upon decomposition of the surface oxide to form a Pd(100) surface can not be investigated within the here described model. As a measure to determine the *onset* of the decomposition of the surface oxide structure the average occupation of the hollow sites by oxygen atoms, $\overline{\Theta}_{\mathrm{O,hol}}$, is evaluated. If the average occupation drops below 90 %, the surface oxide structure is considered as starting to destabilize. This is a rather conservative limit, but it ensures the validity of the kMC model, since up to this coverage a reconstruction of the surface is not expected. Since the average occupation is a global measure over the whole simulation

cell, the situation would be different, though, if a local decomposition of the surface oxide takes place. A decrease in the average occupation of hollow sites by oxygen of 10 % could then correspond to a locally complete decomposition of 10 % of the surface oxide area requiring also a local restructuring of the palladium atoms, instead of indicating the global onset of the decomposition of the complete surface oxide layer. In the present simulations such a local decomposition has not been observed and thus the average occupation, $\overline{\Theta}_{\mathrm{O,hol}}$, appears to be suitable to determine the onset of the surface oxide decomposition.

The simulations are performed for three different temperatures, $T = 300\,\mathrm{K}$, $400\,\mathrm{K}$ and $600\,\mathrm{K}$, and a fixed oxygen pressure of $p_{\mathrm{O_2}} = 1\,\mathrm{atm}$, whereas the CO pressure is increased from 10^{-5} up to $10^{5}\,\mathrm{atm}$. Comparing to the phase diagram in Fig. 8.2 this corresponds to evaluating the stability of the surface oxide along the vertical green arrows marking gas phase conditions of constant oxygen pressure. Starting in the stability region of the surface oxide the CO pressure is increased moving upward towards the stability region of the CO covered Pd(100) surface. Similar to the results discussed in the previous Section, the average surface occupations are evaluated for the system under steady-state conditions. To ensure that the system has reached its steady-state, the simulations are again performed with different initial configurations and the average occupations are calculated over different time intervals.

In Fig. 8.8 the average occupation of hollow sites by oxygen depending on the CO pressure is shown for $T = 300\,\mathrm{K}$. The green line represents the results obtained by using the determined reaction barrier of $\Delta E^{\mathrm{reac}}_{\mathrm{Ohol+CObr}} = 0.9\,\mathrm{eV}$ and $\Delta E^{\mathrm{reac}}_{\mathrm{Obr+COhol}} = 0.5\,\mathrm{eV}$. For CO pressures of $p_{\mathrm{CO}} < 10^{-1}\,\mathrm{atm}$ the surface oxide is clearly stable. If the CO pressure is further increased, the occupation of the hollow sites by oxygen starts to slowly decrease for $p_{\mathrm{CO}} > 10^{-1}\,\mathrm{atm}$. Finally, for CO pressures of $p_{\mathrm{CO}} > 1\,\mathrm{atm}$ the surface oxide is completely destabilized and all hollow sites are then occupied by CO. At $p_{\mathrm{CO}} = 1\,\mathrm{atm}$ the average occupation could not be clearly determined, since under these temperature and pressure conditions the steady-state of the system is rather difficult to define. Due to the rather low temperature of $T = 300\,\mathrm{K}$ the reaction dynamics are much slower than the fast adsorption/desorption dynamics of the CO in bridge sites. Even for the longest simulation times different initial configurations did not converge to the same steady-state. Starting with a configuration, where all hollow sites are filled by oxygen, a reaction process occurs only rather seldom compared to the adsorption/desorption of CO in a bridge site. Nevertheless, the average occupation of the hollow sites by oxygen shows a slow but constant decay with the number of kMC steps. In the longest simulations the average occupation is already less than 90 %, reflecting that under such gas phase conditions the surface oxide clearly starts to decompose. Starting the simulations with a completely empty or randomly filled lattice the average occupation stays below 50 %. Although the exact occupation under steady-state conditions could not be evaluated under these temperature and pressure conditions, the tendency to decompose the surface oxide can already be observed.

To compare the results to the ones obtained within the atomistic thermodynamics approach, the stability region of the surface oxide as determined in the phase dia-

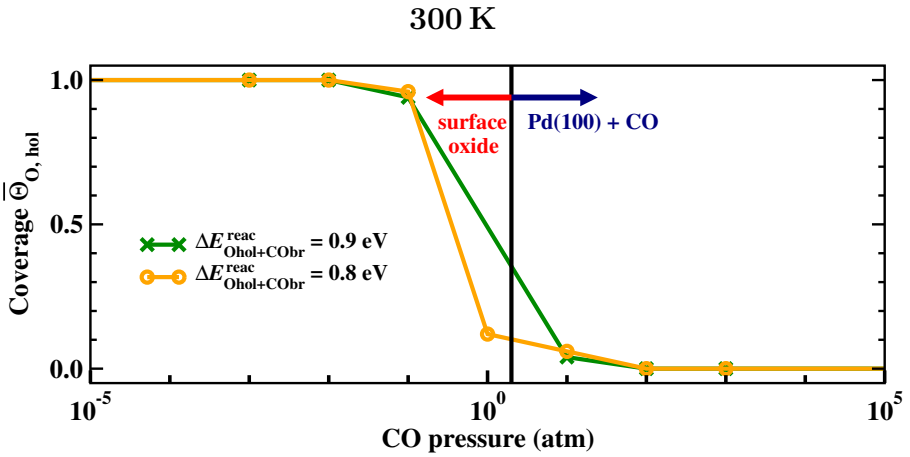

Figure 8.8: Average occupation of hollow sites by oxygen vs. CO pressure for $T = 300\,\mathrm{K}$. The vertical black line marks the boundary between the surface oxide and a CO covered Pd(100) surface as determined within the atomistic thermodynamics approach.

gram is indicated by the vertical black line in Fig. 8.8. Following the green arrow in Fig. 8.2 for $T = 300\,\mathrm{K}$ and $p_{O_2} = 1\,\mathrm{atm}$ starting at a CO pressure of $p_{CO} = 10^{-5}\,\mathrm{atm}$ up to $p_{CO} = 10^{5}\,\mathrm{atm}$ the phase boundary between the surface oxide structure and a CO covered Pd(100) surface is reached for a CO pressure of $p_{CO} \approx 30\,\mathrm{atm}$, i.e. within the atomistic thermodynamics approach the surface oxide will be stable for $p_{CO} \lesssim 30\,\mathrm{atm}$, whereas for $p_{CO} \gtrsim 30\,\mathrm{atm}$ the CO covered Pd(100) surface will be the thermodynamically most stable phase. Running the kMC simulations under these conditions including the ongoing CO_2 formation all of the hollow sites would already be occupied by CO instead of oxygen, clearly indicating that the surface oxide structure would not be stable. Looking again at Fig. 8.8 a depletion of oxygen atoms in hollow sites, and thus the destabilization of the surface oxide structure, starts at already lower CO pressures of $p_{CO} > 10^{-1}\,\mathrm{atm}$, compared to the transition from the stability region of the surface oxide to the one of a CO covered Pd(100) surface in the thermodynamic phase diagram at $p_{CO} \approx 30\,\mathrm{atm}$. This indicates that the stability region of the surface oxide structure is slightly decreased by the ongoing catalytic CO_2 formation.

Since the determined reaction barriers are somewhat approximate, the simulations are also repeated with slightly lower barriers to evaluate the influence on the average surface occupation. Lowering the barrier of the reaction process O bridge + CO hollow by 0.1 eV does not have any effect on the occupation of the different sites. If the barrier of the other reaction process O hollow + CO bridge is reduced to $\Delta E^{reac}_{Ohol+CObr} = 0.8\,\mathrm{eV}$, some slight changes occur, shown by the orange line in Fig. 8.8. Due to the lower reaction barrier the reaction dynamics is somewhat enhanced, i.e. the steady-state of the system can be reached faster. For a CO pressure of $p_{CO} = 1\,\mathrm{atm}$ there are now already 90 % of the hollow sites occupied by CO and only 10 % by

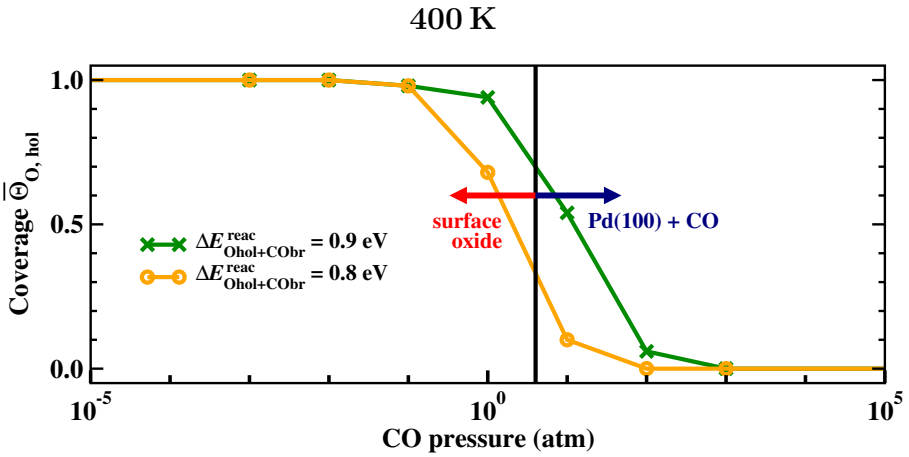

Figure 8.9: Average occupation of hollow sites by oxygen vs. CO pressure for $T = 400\,\mathrm{K}$. The vertical black line marks the boundary between the surface oxide and a CO covered Pd(100) surface as determined within the atomistic thermodynamics approach.

oxygen, but also for this lower barrier the surface oxide structure is clearly stabilized for $p_{CO} < 10^{-1}\,\mathrm{atm}$.

Although the simulations are mainly dominated by the adsorption/desorption processes the consideration of the CO_2 formation at the surface leads thus to a decrease in the stability of the surface oxide compared to the constrained thermodynamic equilibrium results. Diffusion processes are again of minor importance. Simulations performed without considering any diffusion processes show equivalent results. It can be concluded, that under reaction conditions slightly oxygen rich conditions ($p_{O_2}/p_{CO} \approx 10$) are needed to stabilize the surface oxide structure at this temperature.

In Fig. 8.9 equivalent results to Fig. 8.8 are shown for $T = 400\,\mathrm{K}$. The green line represents the results for $\Delta E^{\mathrm{reac}}_{\mathrm{Ohol+CObr}} = 0.9\,\mathrm{eV}$, the orange one for $\Delta E^{\mathrm{reac}}_{\mathrm{Ohol+CObr}} = 0.8\,\mathrm{eV}$, the vertical black line the corresponding boundary between the surface oxide and a CO covered Pd(100) surface in the thermodynamic phase diagram (cf. Fig. 8.2). Compared to the simulations at $T = 300\,\mathrm{K}$ much more reaction processes are detected due to the higher temperature. For CO pressures of $p_{CO} > 10\,\mathrm{atm}$, though, there are almost no reaction processes counted in the steady-state, since here the surface is completely, i.e. both hollow and bridge sites, covered by CO. Yet, this corresponds already to gas phase conditions, where also in a constrained thermodynamic equilibrium the CO covered Pd(100) surface appears as most stable phase (cf. Fig. 8.2). Similar to the results for $T = 300\,\mathrm{K}$ the surface oxide is completely stabilized for CO pressures of $p_{CO} < 10^{-1}\,\mathrm{atm}$. For equal pressures of oxygen and CO (1 atm) and a reaction barrier of $\Delta E^{\mathrm{reac}}_{\mathrm{Ohol+CObr}} = 0.9\,\mathrm{eV}$ there are still 94 % of all hollow sites occupied by oxygen, whereas for the slightly lower barrier of 0.8 eV the occupation is decreased to 68 %. Thus, for this temperature, the stability of the surface oxide under equal pressures of O_2 and CO appears to be rather sensitive to the barrier height.

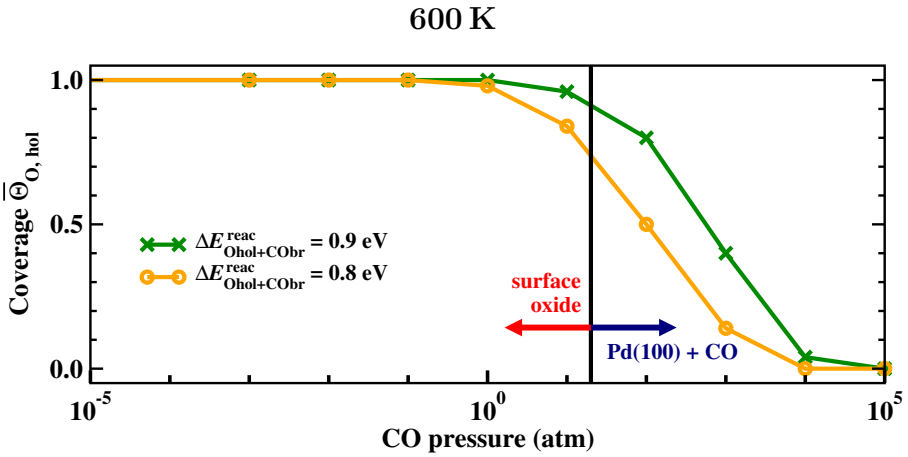

Figure 8.10: Average occupation of hollow sites by oxygen vs. CO pressure for $T = 600\,\mathrm{K}$. The vertical black line marks the boundary between the surface oxide and a CO covered Pd(100) surface as determined within the atomistic thermodynamics approach.

Simulations with an even lower barrier of $\Delta E^{\mathrm{reac}}_{\mathrm{Ohol+CObr}} = 0.7\,\mathrm{eV}$ revealed that the oxygen occupation of hollow sites decreases even further to $\sim 30\,\%$. The uncertainty in the reaction barrier due to the difficulties in finding the transition state, but also due to the choice of the exchange-correlation functional, therefore also introduces an uncertainty in the CO pressure needed to decompose the surface oxide. However, for lower CO pressures of $p_{\mathrm{CO}} < 10^{-1}\,\mathrm{atm}$, the surface oxide is equally stabilized for all three barriers and for CO pressures of $p_{\mathrm{CO}} > 10^{1}\,\mathrm{atm}$ the surface oxide structure is equally destabilized, so that the onset of the surface oxide decomposition can be expected in between CO pressures of $0.1 < p_{\mathrm{CO}} < 10\,\mathrm{atm}$. Considering the uncertainties in the reaction rates and the constraint to a single kMC lattice representing only the surface oxide structure, these results agree rather nicely with the reactor STM experiments by Hendriksen and Frenken [29], where they applied similar temperature and pressure conditions ($T = 408\,\mathrm{K}$, $p_{\mathrm{tot}} = p_{\mathrm{CO}} + p_{\mathrm{O_2}} = 1.23\,\mathrm{atm}$). Depending on the gas phase conditions Hendriksen and Frenken observed a change in the morphology of the surface together with a change in the reaction rate for the CO_2 formation, which was assigned to a change from a metallic to an oxidic phase. It was found that the oxidic phase could only be stabilized under slightly oxygen rich conditions, whereas for an excess of CO the oxidic phase is decomposed by the ongoing CO_2 formation.

The results obtained for an even higher temperature of $T = 600\,\mathrm{K}$ are shown in Fig. 8.10. For this high temperature it is observed, that the surface oxide is actually stable up to rather high CO pressures. Only for CO pressures has high as $p_{\mathrm{CO}} = 10\,\mathrm{atm}$ the decomposition of the surface oxide begins, which is already at the border of its thermodynamic stability. Looking again at the thermodynamic phase diagram in Fig. 8.2 it can be seen that for a temperature of $T = 600\,\mathrm{K}$ and an oxygen pressure of $p_{\mathrm{O_2}} = 1\,\mathrm{atm}$, CO is not stabilized as adsorbate on the surface oxide. Therefore it

is also not readily available as reaction partner and the stability of the surface oxide is hardly influenced by the ongoing reaction. With increasing CO pressure eventually the CO would again be stabilized in the bridge sites, but following the thermodynamic phase diagram this is already in a (T, p)-range, where a CO covered Pd(100) surface would be stable.

8.4 Conclusions

It could be shown that the ongoing catalytic reaction of O and CO to form CO_2 does in fact have some influence on the onset of the surface oxide decomposition. At temperature of $T = 300\,\mathrm{K}$ and $400\,\mathrm{K}$ slightly oxygen-rich conditions are needed to stabilize the surface oxide, whereas in the constrained thermodynamic equilibrium the surface oxide is stable up to and CO excess of 10–30 atm. At a higher temperature of $T = 600\,\mathrm{K}$ the stability of the surface oxide is only very weakly influenced by the ongoing reaction, since under these gas phase conditions CO is not stabilized in an adsorbed state on the surface. These results suggest that under catalytically relevant gas phase conditions of elevated temperatures and ambient pressures the surface oxide structures can actually be stabilized despite the ongoing CO_2 formation and thus might also be a candidate for the catalytically active state of the Pd(100) surface.

If the surface oxide forms under catalytic reaction conditions, then also the reaction rate for the CO_2 formation can be changed compared to the clean surface. Such an effect was also observed in the reactor STM experiments by Hendriksen and Frenken [29]. In going from the smooth metallic Pd(100) surface to a rough oxidic phase a step up in the CO_2 production rate by a factor of 1.5 was observed. Returning to the metal surface led again to a decrease in the reaction rate.

Since in the thermodynamic phase diagram (cf. Fig 7.6) as well as in the kMC simulations the catalytically relevant gas phase conditions appear to be right at the boundary between a CO covered Pd(100) surface and the surface oxide the ongoing catalytic reaction could also lead to a continuous formation and decomposition of the surface oxide structure depending on the local pressure conditions. The oxidation reaction might then not only involve the metal surface or the surface oxide, but might actually induce a change back and forth between the two phases. Thus, in a next step also the transition from the surface oxide to the Pd(100) surface and vice versa would have to be considered in the modeling allowing for a complete decomposition/formation of the surface oxide structure.